Optics Letters

Modal phase-locking in multimode nonlinear optical fibers

Fabio Mangini,[1,†] Mario Ferraro,[1,†*] Yifan Sun,[1] Mikhail Gervaziev,[2,3] Pedro Parra-Rivas,[1] Denis S. Kharenko,[2,3] Vincent Couderc,[4] and Stefan Wabnitz[1,5]

[1] Department of Information Engineering, Electronics, and Telecommunications, Sapienza University of Rome, Via Eudossiana 18, 00184 Rome, Italy
[2] Novosibirsk State University, Pirogova 1, Novosibirsk 630090, Russia
[3] Institute of Automation and Electrometry, SB RAS, Novosibirsk 630090, Russia
[4] Université de Limoges, XLIM, UMR CNRS 7252, 123 Avenue A. Thomas, 87060 Limoges, France
[5] CNR-INO, Istituto Nazionale di Ottica, Via Campi Flegrei 34, 80078 Pozzuoli, Italy
[†] These authors have contributed equally.
*mario.ferraro@uniroma1.it

Received 1 May 2023; revised 16 June 2023; accepted 19 June 2023; posted 20 June 2023; published 3 July 2023

Spatial beam self-cleaning, a manifestation of the Kerr effect in graded-index multimode fibers, involves a nonlinear transfer of power among modes, which leads to robust bell-shaped output beams. The resulting mode power distribution can be described by statistical mechanics arguments. Although the spatial coherence of the output beam was experimentally demonstrated, there is no direct study of modal phase evolutions. Based on a holographic mode decomposition method, we reveal that nonlinear spatial phase-locking occurs between the fundamental and its neighboring low-order modes, in agreement with theoretical predictions. As such, our results dispel the current belief that the spatial beam self-cleaning effect is the mere result of a wave thermalization process.

https://doi.org/10.1364/OL.494543

In multimode optical structures, mode-locking is known to occur via dissipative or nonlinear loss mechanisms. For example, in lasers, the relative phase between longitudinal cavity modes may get locked, so that a short pulse is formed, which experiences reduced losses with respect to a quasi-CW composed by an incoherent mode superposition [1]. By the same argument, in lasers, mode-locking may also occur for transverse cavity modes [2,3], or both longitudinal and transverse modes [4–6].

However, phase-locking among a multiplicity of modes may also appear in purely conservative parametric nonlinear optical processes. The simplest case is provided by the nonlinear coupling between two orthogonal polarization modes in birefringent optical fibers, where the slow mode remains a stable eigenstate, even in the presence of strong Kerr birefringence [7–9]. An example of higher complexity is related to the interaction of a number of waves with different states of polarization, where phase-locked states emerge as stable attractors [10]. In conservative nonlinear multimode systems, e.g., involving counterpropagating waves of different polarizations, mode-locking is of a topological nature, being associated with a minimum of the interaction Hamiltonian of the field [11].

In this work, we reveal that spatial beam self-cleaning (BSC) in graded-index (GRIN) multimode optical fibers [12–15] is a novel manifestation of complex mode-locking, where both mode amplitudes and spatial nonlinear phases remain locked. As a matter of fact, BSC fully preserves the spatial coherence of laser beams [13], even when it is produced by two different GRIN fibers [16]. This leads to an increase of the beam quality or brightness of cleaned beams with respect to speckled beams, a property of utmost importance for many applications, from mode-locked fiber lasers [6] to beam delivery in high-resolution nonlinear imaging [17], to name a few. BSC also leads to a mode power redistribution at the fiber output, in favor of the fundamental mode. The resulting output mode power (or amplitude) distribution can be well reproduced by means of a thermodynamic approach to multimode optical systems, based on the principle of entropy (S) maximization [18–20]. The latter can be written as [21]

$$\mathcal{S} = K \sum_{j=1}^{M} \ln A_j^2, \tag{1}$$

where K denotes the Boltzmann constant, A_j is the amplitude of the jth mode, and M is the number of guided fiber modes. Entropy maximization occurs within the constraints of the conservation of the total power $\mathcal{P} = \sum_j A_j^2$, and the linear part of the Hamiltonian reads $H = \sum_j \beta_j A_j^2$, where β_j is the propagation constant of the jth mode [21]. According to the thermodynamic approach, an equilibrium distribution of A_j is eventually reached after a sufficiently long propagation distance z^*, under the action of weak nonlinearity [19,21,22]. Owing to the latter, the value of z^* is inversely proportional to $\mathcal{P}$, so that BSC is usually demonstrated by varying $\mathcal{P}$ at a fixed fiber length L. In particular, the mode amplitude follows the Rayleigh–Jeans (RJ) law, i.e., the mode amplitudes are fixed, according to [see Fig. 1(a)]

$$A_j^2 = -\frac{KT}{\beta_j + \mu}, \tag{2}$$

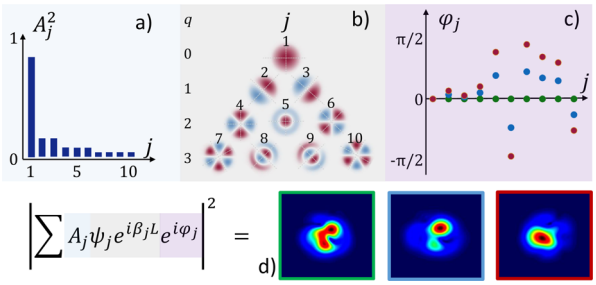

Fig. 1. Spatial mode-locking in GRIN fibers. (a) Mode power distribution according to RJ law [Eq. (2)] with $T = 0.11\,\mathrm{mm}^{-1}$, $\mu + \beta_0 = -51.06\,\mathrm{mm}^{-1}$. (b) Shapes of GRIN fiber mode patterns, Laguerre–Gauss (LG) modes ($\psi_j e^{i\beta_j L}$). The value of the index j for each mode is overlapped to its pattern. (c) Three spatial phase distributions for the first ten modes., (d) Corresponding output beam intensities, using amplitudes A_j in (a) and $L = 3$ m. The beam quality, measured via the correlation between the intensity of the fundamental beam and that of near-field images [26], is 85% (green), 91% (blue), and 97% (red), respectively.

where T and μ denote temperature and chemical potential, respectively. If T is expressed in the same units as the mode propagation constant, then K, which is generally considered a unitary factor, enables the units of T to be transformed to power units.

Now, the thermodynamic approach ignores temporal aspects, and it does not take into account the relative phase among modes. Hence, in this framework, thermalized beams are necessarily incoherent. This is because thermodynamics only involves averaged quantities: at variance with A_j, whose average value is nonzero, the average of the phase is equal to zero, since the latter oscillates between $-\pi$ and π [21,23]. This means that thermodynamics is inherently incapable of describing a main property of BSC, specifically, the robust preservation of spatial coherence, as well as the large beam quality or brightness improvement [6,13,16]. These properties are intrinsically related to the existence of a fixed phase relationship among spatial modes. As a consequence, purely thermodynamic considerations of nonlinear beam propagation are unfit to describe BSC experiments [24].

So one naturally wonders: how can we move beyond thermodynamics, to provide an exhaustive theoretical understanding of BSC? To answer this question, it is necessary to determine the evolution of the nonlinear spatial phase (φ_j), henceforth "phase," which is a challenging task in experiments. Here we do that, by theoretically and experimentally demonstrating that BSC involves a mechanism of power-induced phase-locking among the lowest-order modes, which carry most of the beam power. First, by recalling the linear wave equation, we show that mode amplitude locking leads to a locking of their phases as well. Then, we propose a simple, and yet powerful, numerical approach to determine the values of the mode phases in the occurrence of BSC. All theoretical and numerical results are validated by experiments based on a state-of-the-art holographic mode decomposition (MD) method [25].

Let us first decompose the optical field (Ψ) in a GRIN fiber as

$$\Psi(z,\theta,r) = \sum_{j=1}^{M} c_j(z)\psi_j(\theta,r)e^{-i\beta_j z}, \tag{3}$$

where $\psi_j(\theta,r)$ is the jth guided mode and $c_j(z) = A_j(z)e^{i\varphi(z)}$ is its associated Fourier coefficient. Fig. 1(b) depicts the fiber modes in the LG base. Note that modes are displayed in a triangular shape, to emphasize their degeneracy with respect to the propagation constant $\beta_j = \beta_0 - (q_j + 1)\Delta\beta$, where $\beta_0 = 8937.1\,\mathrm{mm}^{-1}$, $\Delta\beta = 5.5\,\mathrm{mm}^{-1}$, and $q_j + 1 = \lceil(\sqrt{1+8j} - 1)/2\rceil$ is the mode degeneracy, $\lceil\cdot\rceil$ being the ceiling function. In Fig. 1(b), degenerate modes are shown in the same row. Note also that, according to the RJ law [Eq. (2)], degenerate modes have equal amplitudes at thermal equilibrium [cf. bars with equal height in Fig. 1(a)].

To emphasize that mode phase-locking is a crucial ingredient in BSC to increase the beam quality, in Fig. 1(c), we consider three possible sets of values of $\{\varphi_j\}$, i.e., $\varphi_j = 0\ \forall j$ (green dots), experimental values of φ_j, as described in the following (red dots), and intermediate values (blue dots). The intensity profile at a distance $z = L$ is calculated as $|\sum A_j\psi_j e^{i\beta_j L}e^{i\varphi_j}|^2$, with A_j following the RJ law [Eq. (2)], and is shown in Fig. 1(d). As can be seen, the highest beam quality is obtained for the experimental values of φ_j (red framed image); poor spatial quality beams are found otherwise (green and blue framed images).

To derive the mode phase-locking condition, we rely on the Schrödinger equation, i.e., $\partial_z\Psi = -i\hat{H}\Psi$, where $\hat{H}$ is the linear Hamiltonian operator, which, under the hypothesis of weak nonlinearity, simply propagates each mode with its own propagation constant, i.e., $\hat{H}\psi_j(\theta,r) = \beta_j\psi_j(\theta,r)$. Here, we neglect the nonlinear part of $\hat{H}$, which is several orders of magnitude smaller than the linear part of $\hat{H}$ for silica fibers when $\mathcal{P}$ is of the order of tens of kilowatts, i.e., the typical experimental conditions for BSC [18]. Nevertheless, nonlinearity is needed, in concert with linear mode coupling, to enable wave thermalization to the RJ distribution over a relatively short fiber length [27,28]. Hence, we impose the condition that the mode amplitudes reach a steady-state value at $z>z^*$, in agreement with Eq. (2); hence,

$$\partial_z A_j = 0 \quad \forall j \quad \text{at} \quad z>z^*. \tag{4}$$

It has to be noted that Eq. (4), as well as Eq. (2), properly holds for mode amplitudes, which are averaged over a statistical ensemble. Nevertheless, here we identify the average value of A_j with its value within a single experimental realization (e.g., by averaging over the pulse profile). This hypothesis is supported by the fact that BSC experiments are carried out with mode-locked lasers, whose pulses have very little pulse-to-pulse variance. Our method would not hold, instead, for demonstrations of beam cleanup which involve averaging over several realizations with highly different initial conditions, such as in Baudin *et al.* [29].

Whenever nonlinearity can be neglected, locking of the mode amplitude [Eq. (4)] is associated with the locking of its phase as well (this is straightforward to demonstrate, by replacing the derivative of the field [Eq. (3)] with respect to z in the wave equation), i.e., $\partial_z\varphi_j = 0\ \forall j$. This means that, for sufficiently long propagation distances, each mode acquires a z-independent phase, so that, eventually, all modes are locked in phase, i.e.,

$$\partial_z(\varphi_j - \varphi_k) = 0 \quad \forall j,k. \tag{5}$$

Note that such a mathematical derivation does not permit the evaluation of actual steady-state values of the modal phases. These, however, can be determined by recalling some aspects of the thermodynamic theory of BSC. Specifically, we refer to the values of the beam temperature T, which has to be significantly low, to ensure that a sufficiently large amount of the optical power is stored in the fundamental mode at thermal equilibrium.

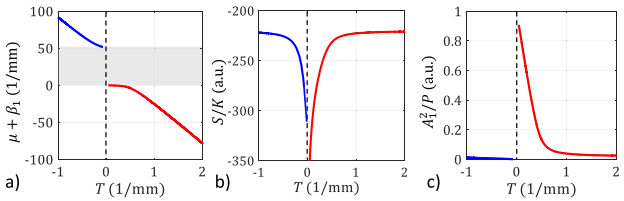

Fig. 2. Thermodynamic parameters for multimode systems at thermal equilibrium, i.e., whenever the mode power distribution obeys a RJ law [19]; input power is set to unity. All plots are as a function of temperature, and for a given GRIN fiber (length and transverse size). (a) Chemical potential. (b) Internal energy. (c) Power fraction of fundamental mode.

Indeed, as a general rule, the lower the temperature, the larger the occupancy of the fundamental mode, i.e., the "cleaner" the beam will be at the fiber output. Indeed, $T = 0$ corresponds to a limit case, which separates the cleanest beams ($T \to 0^+$) from the most speckled beams ($T \to 0^-$), i.e., beams whose occupancy of the higher-order modes (HOMs) is dominant [30,31]. To picture the difference between positive and negative temperatures, in Figs. 2(a) to 2(c), we plot the theoretical dependence of μ, S, and $A_1^2/\mathcal{P}$, respectively, on T [21]. As can be seen, when T approaches zero from the right, μ tends toward the constant value $\mu = -\beta_1$ [see Fig. 2(a)]. Correspondingly, entropy S attains its minimum value, in agreement with the third law of thermodynamics [see Fig. 2(b)]. Finally, as can be seen in Fig. 2(c), the occupancy of the fundamental mode steeply grows toward 1 as $T \to 0^+$, whereas, as $T \to 0^-$, the occupancy of the fundamental mode tends to vanish. Therefore, BSC is associated with a wave thermalization process at low (and positive) temperatures. Indeed, former BSC experiments have shown that the fundamental mode occupancy is always well above 50%. In this case, according to Fig. 2(c), the beam temperature T<0.5 mm^{-1}. This value is comparable to that indicated in Aschieri *et al.* [23] and Baudin *et al.* [29] as the threshold for *wave condensation*.

Such a result is crucial, since it allows us to rely on a variational approach to determine the modal phases at the occurrence of BSC. Indeed, one can reasonably assume that, at $T \simeq 0^+$, the field Ψ is close to the sole fundamental mode ψ_1. Hence, we may treat mode phases as a finite set of variables (ansatz) to be determined, with the constraint that mode amplitudes obey the RJ law [Eq. (2)], to minimize the difference (ε) between the fundamental mode intensity and the output intensity profiles of the total field $\Psi(\theta, r)$, i.e.,

$$\min_{\{\varphi_j\}} \{\varepsilon\} = \min_{\{\varphi_j\}} \left\{ |\Psi(\theta, r)|^2 - \mathcal{P} \cdot |\psi_1(\theta, r)|^2 \right\}. \quad \textbf{(6)}$$

The numerical minimization [Eq. (6)] readily leads to a unique solution, as long as the first few modes are considered: we took the first three degenerate groups, containing the six lowest-order modes, which carry most of the power at thermal equilibrium [see Fig. 1(a)], whereas our numerical routine did not converge when a larger number of modes was taken into account. To compare the predictions of theory with experiments, we used a holographic MD setup, as described by Gervaziev *et al.* [25]. The latter allowed us to retrieve both the mode amplitude and phase of the 78 lowest-order modes, i.e., those belonging to the first 10 groups. Experiments were conducted with an ultra-short pulse laser system pumped by a femtosecond Yb-based laser generating 174 fs pulses with 100 kHz repetition rate at $\lambda = 1030$ nm, with a nearly Gaussian beam shape (M^2=1.3). The laser beam

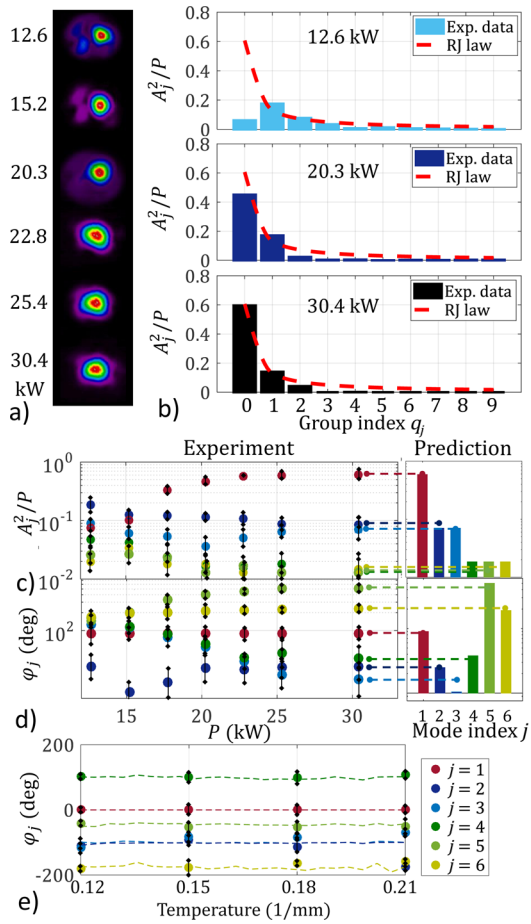

Fig. 3. (a) Experimental beam intensity profile when increasing $\mathcal{P}$. (b) Comparison of corresponding mode power distribution with RJ law. (c), (d) Comparison between experimental data (left) and predictions of Eq. (2) and [Eq. (6)] for the mode amplitude and phase, respectively. (e) Experimental (dots) and numerical (dashedlines) values of modal phase as a function of beam temperature.

was injected at the center of a GRIN fiber with a diameter at $1/e^2$ of peak intensity of 30 μm. We used a 3 m long standard 50/125 GRIN fiber: its core radius, core refractive index along the axis, relative core-cladding index difference, numerical aperture, and fundamental mode radius at $\lambda = 1030$ nm are $r_c = 25$ μm, $n_0 = 1.472$, $\Delta = 0.0103$, NA = 0.2, and $r_{0,0} = 6.33$ μm, respectively. At the fiber output, as usual for BSC, the beam was bandpass filtered at 1030 ± 5 nm, to avoid any loss of coherence owing to spectral broadening. Moreover, as the MD method is based on a spatial light modulator that is polarization sensitive, the beam was projected onto a linear state of polarization by means of a half-wave plate and a polarizer. In this sense, although early works have shown that the state of polarization may drastically change during BSC [32], here we did not analyze the role of light polarization during BSC in a thermodynamic framework. Preliminary results in this regard may be found in Ferraro *et al.* [33].

The experimental results are shown in Fig. 3. We retrieve the mode amplitudes and phases for six different values of the laser pulse peak power. The corresponding beam profiles at the fiber output are shown in Fig. 3(a). As can be seen, at low powers, the output beam is speckled, meaning that thermal equilibrium was

not yet reached, whereas at $\mathcal{P}>23$ kW, speckles transform into a bell shape, and the output beam acquires higher brightness and spatial quality. For the sake of readability, in Fig. 3(b) we report the measured values of the average mode powers ($A_j^2\mathcal{P}$) in each mode degeneracy group as a function of the group index q_j, for only three values of $\mathcal{P}$, i.e., 12.6 kW, 20.3 kW, and 30.4 kW. As can be seen, it is only at the highest power value that the experimental mode powers (bars) agree with the RJ law for $T = 0.11\,\mathrm{mm}^{-1}$ and $\mu + \beta_0 = -51.06\,\mathrm{mm}^{-1}$ (dashed line): in this case, about 60% of the total beam power is carried by the fundamental mode. The values of T and μ were calculated as described in Wu *et al.* [34] and Mangini *et al.* [19].

In Figs. 3(c) and 3(d), we compare experimental measurements of $A_j^2\mathcal{P}$ and φ_j as a function of $\mathcal{P}$ (dots in left panels) with the predictions of Eqs. (2) and (6) (bars in right panels), respectively. As evidenced by the dashed lines, which are a guide for the eye, we found an excellent agreement. Note that modes belonging to the same group, which have almost the same amplitude according to mode power equipartition [23], are nevertheless associated with different phases [cf. the histograms in Figs. 3(c) and 3(d)]. Moreover, it can be noted that the equilibrium values of both A_j and φ_j are progressively reached, as $\mathcal{P}$ grows larger. Indeed, we observed that low-order modes reach a steady phase at lower values of $\mathcal{P}$, when compared with HOMs. Finally, we verified the temperature range of validity of the minimization of ε [Eq. (6)]. We found an excellent agreement between experiments and numerical predictions [see Fig. 3(e)] for $T \lesssim 0.2\,\mathrm{mm}^{-1}$.

In conclusion, we experimentally demonstrated that the coherent nature of spatial BSC in GRIN multimode optical fibers is associated with phase-locking between the fundamental mode and its immediate neighboring low-order modes. The mode phases could be retrieved, along with the relative mode powers, thanks to a holographic MD method based on a phase-only spatial light modulator. Our results conciliate the thermodynamic theory of incoherent wave thermalization with the experimental observation of the preservation of beam spatial coherence in the occurrence of BSC. We envisage that our findings will have a relevant impact on the various potential technological applications of the BSC effect. Specifically, we expect that mode-locking will be strongly reinforced when combining self-cleaning with a dissipative setting, such as in a multimode fiber laser cavity.

Funding. H2020 European Research Council (740355); Ministero dell'Istruzione, dell'Università e della Ricerca (R18SPB8227); Sapienza Università di Roma (AR2221815ED243A0, RG12117A84DA7437); H2020 Marie Skłodowska-Curie Actions (101023717, 101064614, 713694); Agence Nationale de la Recherche (ANR-10-LABX-0074-01, ANR-18-CE080016-01); RSF (21-42-00019).

Acknowledgments. We thank T. Hansson and R. Ferraro for fruitful discussions.

Disclosures. The authors declare no conflicts of interest.

Data availability. Data underlying the results presented in this paper are not publicly available at this time but may be obtained from the authors upon reasonable request.

REFERENCES

1. H. Haus, IEEE J. Sel. Top. Quantum Electron. **6**, 1173 (2000).
2. D. Auston, IEEE J. Quantum Electron. **4**, 420 (1968).
3. B. Fischer, O. Werner, M. Horowitz, and A. Lewis, Appl. Phys. Lett. **58**, 2729 (1991).
4. P. W. Smith, Appl. Phys. Lett. **13**, 235 (1968).
5. L. G. Wright, D. N. Christodoulides, and F. W. Wise, Science **358**, 94 (2017).
6. U. Tegin, B. Rahmani, E. Kakkava, D. Psaltis, and C. Moser, Adv. Photonics **2**, 056005 (2020).
7. B. Daino, G. Gregori, and S. Wabnitz, J. Appl. Phys. **58**, 4512 (1985).
8. H. G. Winful, Opt. Lett. **11**, 33 (1986).
9. K. J. Blow, N. J. Doran, and D. Wood, Opt. Lett. **12**, 202 (1987).
10. G. Millot and S. Wabnitz, J. Opt. Soc. Am. B **31**, 2754 (2014).
11. V. Zakharov and A. Mikhailov, JETP Lett. **46**, 279 (1987).
12. K. Krupa, A. Tonello, A. Barthélémy, V. Couderc, B. M. Shalaby, A. Bendahmane, G. Millot, and S. Wabnitz, Phys. Rev. Lett. **116**, 183901 (2016).
13. K. Krupa, A. Tonello, B. M. Shalaby, M. Fabert, A. Barthélémy, G. Millot, S. Wabnitz, and V. Couderc, Nat. Photonics **11**, 237 (2017).
14. Z. Liu, L. G. Wright, D. N. Christodoulides, and F. W. Wise, Opt. Lett. **41**, 3675 (2016).
15. L. G. Wright, Z. Liu, D. A. Nolan, M.-J. Li, D. N. Christodoulides, and F. W. Wise, Nat. Photonics **10**, 771 (2016).
16. M. Fabert, M. Săpântan, K. Krupa, A. Tonello, Y. Leventoux, S. Février, T. Mansuryan, A. Niang, B. Wetzel, G. Millot, S. Wabnitz, and V. Couderc, Sci. Rep. **10**, 20481 (2020).
17. N. O. Moussa, T. Mansuryan, C.-H. Hage, M. Fabert, K. Krupa, A. Tonello, M. Ferraro, L. Leggio, M. Zitelli, F. Mangini, A. Niang, G. Millot, M. Papi, S. Wabnitz, and V. Couderc, Sci. Rep. **11**, 18240 (2021).
18. H. Pourbeyram, P. Sidorenko, F. O. Wu, N. Bender, L. Wright, D. N. Christodoulides, and F. Wise, Nat. Phys. **18**, 685 (2022).
19. F. Mangini, M. Gervaziev, M. Ferraro, D. Kharenko, M. Zitelli, Y. Sun, V. Couderc, E. Podivilov, S. Babin, and S. Wabnitz, Opt. Express **30**, 10850 (2022).
20. E. Podivilov, F. Mangini, O. Sidelnikov, M. Ferraro, M. Gervaziev, D. Kharenko, M. Zitelli, M. Fedoruk, S. Babin, and S. Wabnitz, Phys. Rev. Lett. **128**, 243901 (2022).
21. F. O. Wu, A. U. Hassan, and D. N. Christodoulides, Nat. Photonics **13**, 776 (2019).
22. M. Zitelli, V. Couderc, M. Ferraro, F. Mangini, Y. S. Rivas, and S. Wabnitz, Photonics Res. **11**, 750 (2023).
23. P. Aschieri, J. Garnier, C. Michel, V. Doya, and A. Picozzi, Phys. Rev. A **83**, 033838 (2011).
24. M. A. Selim, F. O. Wu, G. G. Pyrialakos, M. Khajavikhan, and D. Christodoulides, Opt. Lett. **48**, 1208 (2023).
25. M. Gervaziev, I. Zhdanov, D. Kharenko, V. Gonta, V. Volosi, E. Podivilov, S. Babin, and S. Wabnitz, Laser Phys. Lett. **18**, 015101 (2021).
26. M. Ferraro, F. Mangini, Y. Leventoux, A. Tonello, M. Zitelli, T. Mansuryan, Y. Sun, S. Fevrier, K. Krupa, D. Kharenko, S. Wabnitz, and V. Couderc, J. Lightwave Technol. **41**, 3164 (2023).
27. A. Fusaro, J. Garnier, K. Krupa, G. Millot, and A. Picozzi, Phys. Rev. Lett. **122**, 123902 (2019).
28. O. S. Sidelnikov, E. V. Podivilov, M. P. Fedoruk, and S. Wabnitz, Opt. Fiber Technol. **53**, 101994 (2019).
29. K. Baudin, A. Fusaro, K. Krupa, J. Garnier, S. Rica, G. Millot, and A. Picozzi, Phys. Rev. Lett. **125**, 244101 (2020).
30. K. Baudin, J. Garnier, A. Fusaro, N. Berti, C. Michel, K. Krupa, G. Millot, and A. Picozzi, Phys. Rev. Lett. **130**, 063801 (2023).
31. A. Marques Muniz, F. Wu, P. Jung, M. Khajavikhan, D. Christodoulides, and U. Peschel, Science **379**, 1019 (2023).
32. K. Krupa, G. G. Casta neda, A. Tonello, A. Niang, D. S. Kharenko, M. Fabert, V. Couderc, G. Millot, U. Minoni, D. Modotto, and S. Wabnitz, Opt. Lett. **44**, 171 (2019).
33. M. Ferraro, F. Mangini, R. Jauberteau, M. Zitelli, Y. Sun, P. Parra-Rivas, K. Krupa, A. Tonello, V. Couderc, and S. Wabnitz, Proc SPIE **12407** p. 81 (2023).
34. Y. Wu, H. Pourbeyram, D. N. Christodoulides, and F. W. Wise, Opt. Lett. **46**, 3312 (2021).